On the persistence of cold season SST anomalies associated with the Annular Modes

Laura M. Ciasto[1*], Michael A. Alexander[2], Clara Deser[3] and Matthew H. England[1]

[1] Climate Change Research Centre, University of New South Wales, Sydney Australia

[2]NOAA/Earth System Research Laboratory, Boulder, CO USA

[3]Climate and Global Dynamics Division, NCAR, Boulder, CO USA

Submitted to Journal of Climate

November 18, 2009

*Corresponding author: l.ciasto@unsw.edu.au
Climate Change Research Centre
University of New South Wales
Sydney, NSW 2052
Australia

Abstract

In this study, a simple stochastic climate model is used to examine the impact of the ocean mixed layer depth, surface turbulent energy fluxes and Ekman currents on the persistence of cold season extratropical sea surface temperature (SST) anomalies associated with variability in the annular modes of atmospheric circulation in both hemispheres. Observational analysis reveals that during the cold season, SST anomalies associated with the Southern Annular Mode (SST_{SAM}) persist considerably longer than those associated with the Northern Annular Mode (SST_{NAM}). Using the simple climate model, it is shown that the persistence of the cold season SST_{SAM} is consistent with the simple stochastic climate model paradigm. In the North Atlantic, however, the simple climate model overestimates the persistence of the cold season SST_{NAM}. This overestimate occurs because the NAM-related heat fluxes are not stochastic in time, but rather exhibit negative autocorrelations at lags beyond about 4 weeks. The out-of-phase behavior of the NAM-related heat fluxes may potentially reflect a damping of the NAM-related SST anomalies to the atmosphere.

1. Introduction

The Northern and Southern Annular Modes (NAM and SAM, respectively) are hemispheric-scale patterns of climate variability that explain more of the intraseasonal to interannual variance in the extratropical atmospheric circulation than any other climate phenomena (Thompson and Wallace 2000). These nearly zonally symmetric modes of variability are characterized by north-south vacillations in the midlatitude jet, such that a poleward contraction of the midlatitude jet (i.e., the high index polarity of the annular modes) is associated with anomalous westerlies along 50° latitude and low pressure over the polar regions. It is thought that variability in the annular modes arises from a positive feedback between zonal wind anomalies and baroclinic eddies along the storm tracks in the Northern and Southern Hemispheres (Lorenz and Hartmann 2001, 2003).

The impact of the large-scale patterns of atmospheric variability on the extratropical sea surface temperature (SST) field has primarily focused on Northern Hemisphere Oceans. For example, numerous studies have examined the response of SSTs to variability in the NAM over the North Atlantic sector (also known as the North Atlantic Oscillation; NAO) over the past several decades (e.g., Bjerknes 1964, Kushnir 1994, Marshall et al. 2001, Visbeck et al. 2003, Ciasto and Thompson 2004). These studies demonstrate that, during the positive phase of the NAM/NAO, the associated pattern of SST anomalies is marked by warmer than normal SSTs in the Sargasso Sea surrounded by colder than normal SSTs in the subpolar and subtropical North Atlantic regions (Figure 1, left panel). This meridionally banded structure of SST anomalies, commonly referred to as the North Atlantic tripole, arises primarily from anomalous surface turbulent (latent + sensible) heat fluxes associated with the NAO/NAM (Cayan

1992a, 1992b). In addition, the advection of heat by Ekman currents (hereafter referred to as Ekman heat fluxes) contributes to the structure and magnitude of the resulting SST pattern (e.g., Luksch 1996; Seager et al. 2000; Deser et al., 2009 review paper to appear Dec 11 2009).

Due to a relative lack of *in situ* observations, the response of Southern Ocean SSTs to variability in the SAM has been examined in relatively few studies (e.g., Hall and Visbeck 2002; Lovenduski and Gruber 2005; Sen Gupta and England 2006; Ciasto and Thompson 2008). These studies reveal that during the positive phase of the SAM, the associated pattern of SSTs is characterized by predominantly warm anomalies poleward of 50°S and cold anomalies equatorward of 50°S, except in the central South Pacific where a broad region of enhanced cool SST anomalies is observed (Figure 1, right panel). Similar to the NAM-SST relationship described above, the Southern Ocean SST anomalies associated with the SAM are primarily driven by surface turbulent heat fluxes with a smaller but important contribution from meridional Ekman heat fluxes (Sen Gupta and England 2006; Verdy et al. 2006, Ciasto and Thompson 2008).

The nature in which the extratropical SST anomalies respond to the atmospheric variability is consistent with a general paradigm of large-scale extratropical SST variability first described by Frankignoul and Hasselmann (1977). Within this framework, the ocean mixed layer heat storage rate, or equivalently the tendency in ocean mixed layer temperature, is driven by random atmospheric forcing via surface turbulent heat fluxes and by heat advection due to Ekman currents. The mixed layer temperature anomalies are then damped via surface turbulent heat fluxes. Because the thermal inertia of the ocean mixed layer is relatively large, the resulting tendency in SST is only

sensitive to the low-frequency component of the atmospheric forcing, and thus exhibits a spectrum consistent with red-noise. As a result, the atmospheric forcing, which has a decorrelation time-scale of a few days to weeks, gives rise to SST anomalies with *e*-folding time scales of 3-6 months.

While the paradigm presented by Frankignoul and Hasselman (1977) is consistent with many studies examining the initial decay of year-round extratropical SST anomalies (e.g., Namias et al. 1988; Lau and Nath 1996; Wantanabe and Kimoto 2000; Deser et al. 2003; de Coetlogon and Frankignoul 2003), there are several mechanisms that can further influence the decorrelation time-scales. For example, it has been noted that positive feedbacks between marine stratiform clouds and SSTs can enhance the persistence of SST anomalies during the warm season (Zhang et al. 1998; Norris et al. 1998; Park et al. 2006). Remote forcing of the El Niño/Southern Oscillation (ENSO) has also been shown to have a substantial impact on the persistence of large-scale SST anomalies in the both the North Pacific (Park et al. 2006) and the Southern Ocean (Ciasto and Thompson 2008). In addition, upper ocean processes such as the "reemergence mechanism" where SST anomalies created during winter are stored below the mixed layer in summer and then re-entrained into the mixed layer in the following winter (Namias and Born 1970, 1974; Alexander and Deser 1995; Alexander et al. 1999; Timlin et al. 2002) can further increase the memory of wintertime extratropical SST anomalies to more than one year (Deser et al. 2003).

In this study, we examine the persistence of extratropical SST anomalies associated with the annular modes within the framework proposed by Frankignoul and Hasselman (1977). While the tripole pattern of North Atlantic SST anomalies associated

with the NAO/NAM has been shown to exhibit winter-to-winter persistence via reemergence (de Coetlogon and Frankingoul 2003; Cassou et al. 2007), there has been little research assessing the persistence of the NAM-related SST anomalies within the boreal cold season. In the Southern Ocean, Ciasto and Thompson (2008) briefly examined the relationship between seasonal variations in the depth of the mixed layer and the persistence of SAM-related SST anomalies within the cold season, but they did not consider other mechanisms that could potentially impact the persistence. Here, the goal of the present study is to provide one of the first interhemispheric comparisons between North Atlantic and Southern SST anomalies by examining how the thermal inertia of the ocean mixed layer, as well as the atmospheric forcing and damping, impact the persistence of extratropical SST anomalies associated with the annular modes.

The rest of the paper is outlined as follows. Section 2 documents the data and methods used in this study. In section 3, the observed persistence of SST associated with the annular modes is examined along with the underlying physical mechanisms operating within the framework of the simple climate model. Section 4 examines the extent to which the time-scales of the atmospheric forcing impact the time-scales of the associated SST anomalies and section 5 provides a summary of the key results.

2. Data and Methods

Weekly-mean sea surface temperature data were obtained from the National Oceanic and Atmospheric Science (NOAA) Optimum Interpolation (OI) dataset (Reynolds et al. 2002). The SST data are provided by the NOAA/Office of Oceanic and Atmospheric Research (OAR)/Earth System Research Laboratory (ERSL), Boulder,

Colorado from their website at http://www.cdc.noaa.gov. The OI SST data were derived from a blended objective analysis of both *in situ* and satellite observations and are available on a 1° x 1° latitude-longitude grid from 1981-2008.

Mixed layer depth data are from the Ocean Mixed Layer Depth Climatology Dataset as described in de Boyer Montegut et al. (2004). The data are available in monthly format on a 2° x 2° latitude-longitude mesh and were derived from over five million individual vertical profiles measured between 1941 and 2008, including data from Argo profilers, as archived by the National Oceanographic Data Center (NODC) and the World Ocean Circulation Experiment (WOCE). The depth of the mixed layer is defined as the upper-most depth at which temperature differs from the temperature at 10 m by 0.2 °C.

The geopotential height and surface turbulent (latent + sensible) heat flux data are from the National Centers for Environmental Prediction-National Center for Atmospheric Research (NCEP/NCAR) reanalysis (Kalnay et al. 2001) available from the NOAA/OAR/ESRL Physical Sciences Division (PSD). The NCEP/NCAR reanalysis data are gridded on a 2.5° x 2.5° latitude-longitude mesh. Heat advection by Ekman currents were calculated using wind stress measurements derived from the NCEP/NCAR reanalysis. It should be noted that there are known biases in the NCEP/NCAR reanalysis turbulent heat flux data (Josey et al. 2001; Smith et al. 2001; Yu and Weller 2004); other climatologies such as the Southampton Oceanography Centre (SOC; Josey et al. 1998) and the Comprehensive Ocean-Atmosphere Data Set (COADS; da Silva et al. 1994) are more often used in the North Atlantic. However, the SOC and COADS data are both derived from *in situ* observations of which there are relatively few in the Southern Ocean,

particularly poleward of 50°S. Hence the NCEP/NCAR reanalysis turbulent heat fluxes, which are part of a global reanalysis employing a data assimilation system, have improved spatial coverage. Furthermore, the reanalysis heat fluxes have been shown to correspond well with the observed SST anomalies associated with large-scale atmospheric circulation variability in the North Atlantic (e.g., Deser and Timlin 1997) and Southern Oceans (Sen Gupta and England 2006; Screen et al. 2009).

The SAM and NAM indices were obtained from the NOAA Climate Prediction Center (CPC). Daily mean values of the SAM (NAM) are found by projecting daily 700-mb (1000-mb) height anomalies poleward of 20° onto the leading empirical orthogonal function of monthly-mean 700-mb (1000-mb) heights, calculated for the period 1979-2000. The high index polarity of the NAM and SAM are characterized by negative height anomalies over the pole surrounded by positive height anomalies at ~45°-55°. Both indices were standardized by subtracting the long-term mean and dividing by the long-term standard deviation. Note that the indices of the NAM, which corresponds to the leading pattern of Northern *Hemisphere* atmospheric variability, and the NAO, which corresponds to the leading pattern of North *Atlantic* atmospheric variability, are highly correlated at 0.89 (Hurrell et al. 2003). Furthermore, in this study, the analyses based on the NAM index were repeated using the NAO index and the results of these analyses were not sensitive to the choice of index.

In this study, we make extensive use of autocorrelation analyses to examine the persistence of extratropical SST anomalies associated with the annular modes. Statistical significance of the correlation coefficients is assessed using a one-tailed Student *t-test* based on an effective sample size determined from the method outlined in Bretherton et

al. (1999). The results presented here are divided into the warm season, corresponding to November-April in the Southern Ocean and May-October in the North Atlantic, and cold season, corresponding to May-October in the Southern Ocean and November-April in the North Atlantic. Before calculating the autocorrelations, the data were first detrended to avoid "reddening" related to long-term trends. Furthermore, the cold tongue index (i.e., SST anomalies averaged over the region 5°S-5°N, 170°-120°W) was linearly regressed from the data to avoid persistence in SST anomalies associated with the low-frequency variability inherent in ENSO. While linear regression of the cold tongue index from the data removes a large fraction of the SST persistence related to ENSO variability (Ciasto and Thompson 2008), there is likely to be some residual influence of ENSO. However, ENSO is only significantly correlated to SAM/NAM variability over the Southern Hemisphere and only during its warm season (L'Heureux and Thompson 2006) and linear regression of ENSO from Southern Ocean cold season data and North Atlantic warm and cold season data had little impact on the results during those seasons.

3. Autocorrelations of observed and simulated SST anomalies associated with the annular modes

The top panel of Figure 2 shows the autocorrelation functions of the observed year-round expansion coefficient time series of the North Atlantic SST anomalies associated with the NAM (blue line; hereafter referred to as SST_{NAM}) and the Southern Ocean SST anomalies associated with the SAM (black line; hereafter referred to as SST_{SAM}). The expansion coefficient time series were formed by projecting weekly mean North Atlantic (Southern Ocean) SST anomalies onto maps of North Atlantic (Southern

Ocean) SST anomalies regressed onto standardized values of the NAM (SAM) shown in Figure 1.

When all seasons are considered, the autocorrelations of SST_{SAM} (~0.5) remain statistically significant within the first three months, but SST_{NAM} exhibit less persistence, decaying to ~0.2 over the same period. A subdivision of the data into warm and cold seasons (Figure 2, bottom panel) reveals that during the warm season, there exist negligible differences between the autocorrelation functions of the SST_{SAM} and SST_{NAM}, both decaying to ~0.3 after three months. During the cold season, the autocorrelation curve of SST_{NAM} continues to exhibit a rapid decay, but SST_{SAM} features a considerably higher degree of persistence, characterized by correlations of ~0.7 after three months. The results in Figure 2 are not sensitive to small changes (±4 weeks) in the definition of the warm and cold seasons. Furthermore, similar results were obtained when the analysis was repeated separately on the first and second halves of the seasonal time periods.

In the following analysis, the simple stochastic climate model described in Frankignoul and Hasselman (1977; hereafter referred to as FH77) is used to explore how atmospheric forcing and damping of SST anomalies, as well as its influence on ocean mixed layer depth, control the persistence of extratropical SST anomalies associated with the NAM and the SAM. The analysis focuses primarily on the cold season when the interhemispheric differences in SST persistence are largest. The governing equation for the FH77 model is:

$$\rho c_p H \frac{dT'}{dt} = F' - \lambda T' \qquad (1)$$

where ρ is the density of seawater (1000 kg m^{-3}), c_p is the heat capacity of the ocean (4218 J kg^{-1} K^{-1}), H is the depth of the ocean mixed layer, T' is the temperature anomaly,

F' represents the atmospheric forcing and λ corresponds to the linearized damping parameter which represents the damping of *T'* back to atmospheric temperature via turbulent heat fluxes.

The ocean mixed layer depths are taken to be 70 m and 115 m, corresponding to the climatological mean cold season mixed layer depth averaged across the North Atlantic (H_{NA}; 20°-80°N, 90°W-30°E) and Southern Oceans (H_{SO}; 20°-80°S 0°-360°E), respectively. The North Atlantic and Southern Ocean mixed layer depth averages are weighted by the regression coefficient between the NAM and North Atlantic SST anomalies and between the SAM and Southern Ocean SST anomalies at each grid point, respectively, to emphasize the regions impacted most by the annular modes.

The damping coefficient λ is given as 25 $Wm^{-2}\,K^{-1}$ in both the North Atlantic and Southern Ocean basins and was chosen based on previous studies that have demonstrated values of λ ranging from 15-35 $Wm^{-2}\,K^{-1}$ during the Northern Hemisphere cold season (Barsugli and Battisti 1998, Frankignoul et al. 1998, Deser et al. 2003, and Park et al. 2005). A relative lack of *in situ* observations has limited calculations of λ in the extratropical Southern Hemisphere, although Park et al. (2005) estimate values in the range 15-35 $Wm^{-2}\,K^{-1}$ equatorward of 40°S, consistent with those calculated in the North Atlantic.

The model in Eq. (1) is first used to determine if the differences in the depth of the ocean mixed layer, which is somewhat shallower in the North Atlantic than in the Southern Ocean, can explain the observed differences in the persistence in the cold season

SST_{SAM} and SST_{NAM}. To isolate the influence of the mixed layer depth, the forcing F' is specified as a white noise time series. Because white noise is by definition uncorrelated with itself at all lags except zero, the autocorrelation function (r) of T' of Eq. (1) can be written as a function of lag (τ):

$$r(\tau) = e^{-\lambda\tau/\rho c_p H} \tag{2}$$

Eq. (2) demonstrates that the autocorrelation function of temperature T' is exponentially dependent on the mixed layer depth H (i.e., the thermal inertia of the ocean mixed layer) and λ the rate at which T' is damped back to atmospheric temperature via surface turbulent heat fluxes. The formulation of the FH77 model represented by Eq. (2) is hereafter referred to as the "white noise model".

In the first case, λ is assumed to be the same in both the North Atlantic and Southern Oceans (λ=25 Wm^{-2} K^{-1}) and thus the autocorrelation functions of T' are only dependent on H_{NA} and H_{SO}. Figure 3 shows the theoretical autocorrelation curves derived from Eq. (2) for λ=25 Wm^{-2} K^{-1} and H_{NA} (dashed blue line) and H_{SO} (dashed black line). Consistent with Ciasto and Thompson (2008), the theoretical decay of T' based on H_{SO} exhibits strong agreement with the observed cold season SST_{SAM}. However, there is considerably less agreement between the theoretical and observed autocorrelation functions in the North Atlantic. While the mixed layer in the North Atlantic is shallower than the Southern Ocean, the theoretical autocorrelation function derived using H_{NA} decays only slightly faster than the function derived using H_{SO}. As a result, the theoretical

autocorrelation function based upon H_{NA} drastically overestimates the persistence of the cold season SST_{NAM}.

The estimate of H_{NA} is a simplified representation of the ocean mixed layer depth over the North Atlantic Ocean, as H_{NA} was calculated by averaging over several months and across large regions, aliasing mixed layer depths ranging from less than 50 m in the Sargasso Sea and subtropical regions to well over 400 m in the subpolar regions (not shown). However, in order to produce a theoretical autocorrelation function that exhibits reasonable agreement with that of the observed cold season SST_{NAM}, the assumed mixed layer depth H_{NA} would have to have been set to ~25 m, a depth that is considerably shallower than observations across much of the North Atlantic basin during the boreal cold season.

To determine the impact of the damping coefficient λ on the persistence of SST anomalies, Eq. (2) is solved for a range of $\lambda = 20 - 30$ Wm^{-2} K^{-1}. According to Eq. (2), the autocorrelation function of T' is inversely proportional to λ such that, assuming that H is constant, increased damping to the atmosphere will give rise to decreased persistence of the ocean temperature anomalies. The results reveal that changing the damping coefficient only slightly modifies the theoretical autocorrelation function derived using H_{SO} (Figure 3, light grey shading). The theoretical autocorrelations based on H_{NA} are also only marginally reduced as λ increases and still drastically overestimates the persistence of the observed cold season SST_{NAM} (Figure 3, light blue shading). In order to generate a theoretical autocorrelation function similar to the observations (assuming $H = H_{NA}$), the damping

parameter λ would have to be 65-70 $Wm^{-2}\,K^{-1}$, a value that is well outside the observed range (Frankignoul et al. 1998; Park et al. 2005).

The analysis above assumes that the surface turbulent and Ekman heat fluxes associated with the annular modes have little-to-no memory and can be approximated as stochastic in time. This assumption is assessed now by solving Eq. (1) for T' using the same values of λ, H_{SO}, and H_{NA} as in the white noise model above, but F' is now defined as the sum of the observed cold season surface turbulent (sensible + latent) and Ekman heat fluxes associated with the NAM and the SAM. This formulation of the FH77 model in Eq. (1) is hereafter referred to as the "observed heat flux model". Note that while the surface radiative heat fluxes associated with the annular modes are not included in this heat flux formulation; previous studies have noted the impact of radiative heat fluxes on the persistence of warm season SST anomalies (Norris et al. 1998; Park et al. 2005). However, the results described below remain virtually unchanged when the radiative heat fluxes, which exhibit one-third of the amplitude of the surface turbulent heat fluxes, were considered. We thus hereafter analyze the "observed heat flux model" with radiative heat flux terms ignored.

When Eq. (1) is forced with the observed surface turbulent and Ekman heat fluxes associated with the SAM, the resulting theoretical autocorrelations (Figure 4; black dashed curve) yield approximately the same degree of persistence as the autocorrelation function derived from the white noise model (i.e., compare the black dashed curves in Figs. 3 and 4) and thus still exhibits good agreement with the cold season SST_{SAM}. However, the theoretical T' derived using the observed NAM-related fluxes and H_{NA} (Figure 4; blue dashed curve) now decays such that the associated autocorrelations

decrease to ~0.2 within the first 3 months, which is considerably faster than the decay derived from the white noise model (i.e., compare the blue dashed curves in Figs. 3 and 4) and now shows improved agreement with the observed decay of the cold season SST_{NAM}. Similar to the results from the white noise model, the theoretical autocorrelation functions derived from the observed heat flux model are not strongly sensitive to the feedback parameter λ in of 20-30 $Wm^{-2}K^{-1}$. While the observed heat flux forcing includes both a forcing and a feedback component, the feedback component is likely to be relatively small on the time scales analyzed here (i.e., less than three months).

The robustness of the results in Figs. 3 and 4 is tested by examining the persistence of observed area-averaged SST anomalies associated with the NAM and SAM on smaller regional scales. Figure 5 shows the observed autocorrelation functions of area-averaged cold season SST anomalies for the following three regions impacted by the NAM: the subpolar North Atlantic (40°-50°N, 30°-50°W; top panel), the Sargasso Sea (30°-40°N, 55°-75°W; middle panel) and the subtropical North Atlantic (20°-30°N, 20°-40°W; bottom panel). Also plotted in Figure 5 are the theoretical autocorrelation functions derived from Eq. (2) (white noise model; dashed red line) and derived from Eq. (1) with F' specified as the observed total heat flux (i.e., the observed heat flux model; blue dashed line).

The results in Figure 5 reveal that the temporal behavior of regional scale area-averaged cold season North Atlantic SST anomalies is broadly consistent with that of the basin-wide SST projections onto the NAM. Similar to SST_{NAM}, the observed area-averaged SST anomalies in the three regions of the North Atlantic experience rapid decay to ~ 0.2 - 0.3 within the first three months. Because the average cold season mixed layer

depths in these regions range from 70-80 m in the subtropical and Sargasso Sea regions to 110 m in the subpolar North Atlantic, the theoretical autocorrelation functions of T' derived from the white noise model, which is dependent only on H, largely overestimate the persistence of the SST anomalies in all three regions. The theoretical autocorrelation functions derived from the observed heat flux model, which is dependent on the observed surface turbulent and Ekman heat fluxes as well as on H, provides a better estimation of the observed SST autocorrelations, particularly in the subpolar North Atlantic.

In the Southern Ocean, four regions impacted by the SAM were chosen: the Central Pacific (45°-60°S, 120°-140°W), the western Pacific (35°-50°S, 170°E-170°W), the Central Indian Ocean (35°-50°S, 80°-100°E) and the South Atlantic (40°-55°S, 15°-35°W). The area-averaged cold season SST anomalies in the two Pacific sectors exhibit relatively long decorrelation time scales (Figure 6), similar to the basin wide Southern Ocean SAM-related SST anomalies. There is also strong agreement between the theoretical T' derived from the white noise model and that derived from the observed heat flux model. In the South Atlantic, the area-averaged SST anomalies, which are less persistent than the cold season SST_{SAM}, exhibit reasonable agreement with the results obtained from the observed heat flux model, but the theoretical autocorrelation function is somewhat underestimated by the white noise model. A notably different situation is observed in the Indian Ocean where the area-averaged SST anomalies are largely over-estimated by the theoretical autocorrelations of T' derived from either the white noise or the observed heat flux models. One possible explanation for this is that the depth of the mixed layer has been overestimated in the Indian Ocean, a region that has limited *in situ* observations available to calculate the mixed layer depth. However it is also possible that

the simple formulation of Eq. (1) is not sufficient to capture the persistence of SST variability in the Indian Ocean, and that neglected mechanisms such as mean advection by ocean currents, eddies, and/or ocean mixed layer processes play a role.

4. Lagged analysis of the atmospheric circulation associated with the annular modes

The results from the previous section suggest that the persistence of Southern Ocean SST anomalies associated with the SAM can be largely determined by the thermal inertia of the ocean mixed layer, whereas the persistence of the North Atlantic SST anomalies appears to be further impacted by *deviations of* the observed surface turbulent and Ekman heat fluxes *from white noise*. In this section, we further examine the atmospheric forcing associated with the annular modes and the extent to which it affects the persistence of the resulting SST anomalies. Figure 7 shows the autocorrelation functions of the surface turbulent heat fluxes associated with the SAM and NAM (top panel) as well as the NAM- and SAM-related Ekman heat fluxes (middle panel) and the total (i.e., turbulent + Ekman) heat fluxes (bottom panel). For both the NAM and the SAM, the autocorrelation functions of the turbulent heat fluxes are similar to those of the Ekman heat fluxes. However, the amplitude of the surface turbulent heat fluxes are approximately twice that of the Ekman heat fluxes (not shown), and thus the detailed structure of the autocorrelation functions of the total heat fluxes primarily reflects the persistence of the surface turbulent heat fluxes.

The bottom panel of Figure 7 reveals that the autocorrelation function of the total heat fluxes is similar over the first two weeks, but the NAM-related heat flux autocorrelations are consistently lower than those associated with the SAM between

weeks 2 and 9. During that time, the SAM-related heat fluxes remain significantly correlated at the 95% confidence level ($r > 0.1$) whereas the NAM-related heat fluxes become weakly but significantly negatively correlated at ~7 weeks, indicating that the NAM-related heat fluxes change sign after approximately 1-2 months. However, the SAM and the NAM (or NAO) indices do not exhibit the same differences in persistence as shown in the heat fluxes. The autocorrelation functions of the NAM and SAM (not shown) are very similar at all lags during the cold season, both exhibiting e-folding time scales of 1-2 weeks and neither indices exhibit negative autocorrelations.

The evolution of the heat fluxes associated with the annular modes is also illustrated in Figures 8 and 9, which show the regressions of surface turbulent+Ekman heat fluxes (shading) and 1000-hPa height (Z_{1000}; contours) anomalies onto the annular modes at lags ranging from 1 to 9 weeks (i.e. total heat fluxes and Z_{1000} lag annular modes). In the North Atlantic, the pattern of total heat flux anomalies associated with the positive phase of the NAM (Figure 8) decays within the first 3 weeks as the overlying atmospheric circulation weakens. However, by lags of 5 – 7 weeks, the heat flux anomalies have reversed sign, now resembling the opposite phase of the NAM. Although it is expected that the heat flux anomalies should reverse sign as the SST anomalies damp back to the atmospheric temperature (Barsugli and Battisti 1998; Frankignoul et al. 1998), the evolution of atmospheric circulation anomalies may also contribute to the lagged heat flux anomalies. For example, the now-positive fluxes along 45º-55ºN appear to be consistent with the southerly winds that arise from the contraction and slight poleward shift of the positive height anomalies in the Eastern Atlantic. Similarly, the cyclonic circulation anomaly that develops in the southwestern portion of the Atlantic

basin at lags 5-7 weeks may contribute to the negative heat flux anomalies in the Sargasso Sea and positive flux anomalies along 25ºN. Whether the cyclonic circulation anomaly represents a dynamical response of the atmosphere to the NAM-induced SST anomaly pattern, or is an inherent feature of the decay of the NAM, remains to be determined. Qualitatively similar results were obtained when the regression analysis was repeated using the NAO index. In the Southern Ocean, the overall structure of the atmospheric circulation associated with the positive phase of the SAM also weakens with in the first few weeks but the negative height anomalies west of the Antarctic Peninsula and the positive height anomalies over New Zealand tend to persist for several weeks. The underlying surface turbulent and Ekman heat fluxes also exhibit some persistence through the first 3-5 weeks but do not change sign in the subsequent lags.

The results in Figs. 7 -9 suggest at least two possible scenarios through which the surface turbulent and Ekman heat fluxes related to the annular modes could impact the persistence of the associated SST anomalies:

1) The relatively high persistence of the SAM-related fluxes in turn increases the persistence of the resulting SAM-related SST anomalies.

Because the surface turbulent and Ekman heat fluxes associated with the SAM exhibit variability that persists significantly longer than white noise, it is possible that the resulting SST anomalies reflect this increased persistence in atmospheric forcing. This possibility is tested using a 1st order Markov model, namely:

$$F(t) = \sum_{i=1}^{N} aF(t-i) + (1-a^2)\varepsilon(t) \qquad (3)$$

where *a* corresponds to the lag-one autocorrelation that measures the memory at a previous time *t*, and ε is the white noise time series. According to Eq. (3), the *e*-folding time scale (i.e., the persistence) of the time series *F* increases as the lag-one autocorrelation *a* increases.

For a range of *e*-folding time scales from 1 to 13 weeks, the model in Eq. (3) is used to calculate *F,* which is then used in Eq. (1) to solve for T' using $H = 75$ m and $\lambda = 25$ $Wm^{-2}K^{-1}$. Figure 10 demonstrates that the *e*-folding time scale of T' increases monotonically as the e-folding time scale of the atmospheric forcing *F* also increases. However, the e-folding time-scale of T' only increases by a few weeks when the e-folding time scale of the atmospheric forcing increases from 0 (i.e. white noise) to 1-2 weeks (the *e*-folding time scale of SAM-related fluxes), which suggests that describing the SAM-related fluxes as white noise is a reasonable first-order approximation. Qualitatively similar results are obtained when the analysis in Figure 10 is repeated using other physically reasonable mixed layer depths.

2) The out of phase persistence of the NAM-related fluxes in turn decreases the persistence of the resulting NAM-related SST anomalies.

Figures 7 and 8 show that the North Atlantic surface turbulent and Ekman heat fluxes become negatively correlated with the NAM after 1-2 months, thus acting in the opposite sense of the initial heat fluxes that generated the SST anomalies. Consequently, the NAM-related SST anomalies as well as the initial heat fluxes may be attenuated by the out-of-phase heat flux anomalies at a rate faster than if the out-of-phase heat fluxes were absent. That the NAM-related fluxes are not stochastic in time could explain why

the white noise model over-predicts the persistence of the cold season NAM-related SST anomalies.

5. Summary

This study provides one of the first comparisons of the large-scale extratropical SST variability between the North Atlantic and Southern Ocean basins, focusing on the persistence of these SST anomalies associated with the annular modes. The initial analysis reveals that during the warm season, observed North Atlantic SST anomalies associated with the NAM and Southern Ocean SST anomalies associated with the SAM exhibit similar degrees of persistence. In contrast, during the cold season, the NAM-related SST anomalies decay considerably faster than the SAM-related SST anomalies, which remain significantly correlated after 3 months. Possible mechanisms that can account for the observed differences in the persistence of cold season SST anomalies were examined within the context of the simple stochastic climate model proposed by FH77. In this idealized model, the tendency in SST anomalies is driven by an atmospheric forcing, characterized by surface turbulent and Ekman heat fluxes, damped back to atmospheric temperatures via surface turbulent heat fluxes, and inversely proportional to the depth of the ocean mixed layer. We analyzed two versions of the formulation outlined in FH77 to explore the persistence of extratropical SST anomalies: 1) the theoretical autocorrelations of T' were derived using mixed layer depths representative of the North Atlantic and Southern Ocean cold seasons, and the atmospheric forcing F' was modeled as a white noise time series (i.e., the "white noise" model) and 2) the theoretical autocorrelations of T' were derived using the same mixed

layer depths as in 1) but the forcing F' was defined as the observed surface turbulent and Ekman heat fluxes associated with the annular modes (i.e., the "observed heat flux" model).

In the Southern Ocean, the persistence of the observed cold season SST_{SAM} is well-estimated by the simple climate model when the atmospheric forcing is approximated as white noise and the ocean mixed layer depth is taken to be the climatological mean cold season value averaged across the Southern Ocean. Forcing the model with observed SAM-related turbulent and Ekman heat fluxes yields qualitatively similar results. Furthermore, changing the feedback parameter λ had a relatively small effect on the theoretical autocorrelations. The autocorrelation analysis of the SAM-related total heat fluxes demonstrates that they exhibit significantly more memory than a white noise process, but the fluxes do not significantly increase the persistence of the resulting SST anomalies. This suggests that prescribing the heat flux forcing of Southern Ocean SST anomalies as a white noise process is a reasonable first-order approximation. Similar results were obtained when the analysis is repeated over smaller area-averaged regions of the Southern Ocean, although the idealized FH77 model does not capture the observed cold season SST persistence in the Indian Ocean.

In the North Atlantic, the average cold season mixed layer depths are somewhat shallower than in the Southern Ocean, but nevertheless the white noise model drastically overestimates the persistence of the NAM-related SST anomalies, suggesting that the forcing is not stochastic in time. When the model is forced with the observed surface turbulent and Ekman heat fluxes associated with the NAM, the resulting theoretical autocorrelation function is more comparable to that of the observed cold season SST_{NAM}.

Analysis of the lagged relationship between the NAM and the associated heat fluxes reveals that the fluxes exhibit an out-of-phase pattern after 1-2 months, which may contribute to the accelerated damping of the NAM-related SST anomalies as well as the NAM-related heat fluxes themselves. There is some evidence to suggest that the evolution of the heat fluxes is consistent with temporal changes in the overlying circulation, but may also reflect a damping of the NAM-related SST anomalies to the overlying atmospheric temperature field.

In this study, the persistence of extratropical SST anomalies was diagnosed using a simple formulation in which the ocean is treated as a slab mixed layer with fixed depth *H* coupled to the atmosphere. By doing so, several key mechanisms have been excluded that may impact on our results, including coupled air-sea feedbacks, which Barsugli and Battisti (1998) demonstrate increase persistence due to a reduction in thermal damping. Advection by mean ocean currents has also been neglected, and this can act to increase the persistence of SST anomalies (de Coetlogon and Frankignoul 2003). Furthermore, our analysis does not account for variations in the damping parameter λ. Several studies have also shown that splitting λ into two components: a constant and a stochastically varying component that rapidly varies with the wind speed can impact the time-scales of the resulting SST variability (Sura et al. 2006; Sura and Newman 2008).

Another simplification of the idealized climate model is the use of a fixed mixed layer depth, which does not allow for re-entrainment of SST anomalies due to deepening of the mixed layer during fall/winter (Deser et al. 2003). This entrainment of SST anomalies from the previous spring could affect the persistence of SST in the subsequent cold season, particularly if the re-entrained SST anomalies are out of phase with those

initiated in the cold season. The results presented in this study did not change significantly when a weekly varying climatological mean mixed layer depth was used. However, future work should investigate a full entraining model, which takes account of varying mixed layer depths as well as explicitly including SST anomalies from the previous spring.

References:

Alexander, M.A., and C. Deser, 1995: A mechanism for the recurrence of wintertime midlatitude SST anomalies. *J. Phys. Oceanog.*, **25**, 122–137.

Alexander, M.A., C. Deser, and M.S. Timlin, 1999: The reemergence of SST anomalies in the North Pacific Ocean. *J. Climate*, **12**, 2419–2433.

Barsugli, J.J., and D.S. Battisti, 1998: The Basic Effects of Atmosphere–Ocean Thermal Coupling on Midlatitude Variability. *J. Atmos. Sci.*, **55**, 477–493.

de Boyer Montégut, C., G. Madec, A. S. Fischer, A. Lazar, and D. Idicone, 2004: Mixed layer depth over the global ocean: An examination of profile data and a profile-based climatology. *J. Geophys. Res*., **109**, C12003, doi:10.1029/2004JC002378.

Bjerknes, J., 1964: Atlantic air-sea interaction, *Adv. Geophys.,* **10**, 1-82.

Bretherton, C.S., M. Widmann, V.P. Dymnikov, J.M. Wallace, and I. Bladé, 1999: The Effective Number of Spatial Degrees of Freedom of a Time-Varying Field. *J. Climate*, **12**, 1990–2009.

Cassou C., C. Deser, and M. A. Alexander, 2007: Investigating the impact of reemerging sea surface temperature anomalies on the winter atmospheric circulation over the North Atlantic. *J. Climate*, **20**, 3510–3526.

Cayan, D. R., 1992a: Latent and sensible heat-flux anomalies over the northern oceans: the connection to monthly atmospheric circulation. *J. Climate,* **5**, 354-369.

Cayan, D. R., 1992b: Latent and sensible heat-flux anomalies over the northern oceans: driving the sea surface temperature. *J. Phys. Oceanogr*., **22**, 859-881.

Ciasto, L.M., and D.W.J. Thompson, 2004: North Atlantic Atmosphere–Ocean Interaction on Intraseasonal Time Scales. *J. Climate*, **17**, 1617–1621.

Ciasto, L.M., and D.W.J. Thompson, 2008: Observations of Large-Scale Ocean–Atmosphere Interaction in the Southern Hemisphere. *J. Climate*, **21**, 1244–1259.

de Coëtlogon, G., and C. Frankignoul, 2003: The Persistence of Winter Sea Surface Temperature in the North Atlantic. *J. Climate*, **16**, 1364–1377.

da Silva, A. M., C. C. Young, and S. Levitus, 1994: *Algorithms and Procedures.* Vol. 1, *Atlas of Surface Marine Data,* NOAA Atlas Series, 74 pp.

Deser, C., and M.S. Timlin, 1997: Atmosphere–Ocean Interaction on Weekly Timescales in the North Atlantic and Pacific. *J. Climate*, **10**, 393–408.

Deser, C., M. A. Alexander, and M. S. Timlin, 2003: Understanding the persistence of sea surface temperature anomalies in midlatitudes. *J. Climate,* **16**, 57-72.

Deser, C., M. A. Alexander, S. -P. Xie, and A. S. Phillips, 2009: Sea surface temperature variability: patterns and mechanisms. *Ann. Rev. Mar. Sci.*, in press.

Frankignoul, C., and K. Hasselman, 1977: Stochastic climate models. Part II: Application to sea-surface temperature variability and thermocline variability. *Tellus*, **29**, 289-305.

Frankignoul, C., A. Czaja, and B. L'Heveder, 1998: Air–Sea Feedback in the North Atlantic and Surface Boundary Conditions for Ocean Models. *J. Climate*, **11**, 2310–2324.

Hall, A., and M. Visbeck, 2002: Synchronous variability in the Southern Hemisphere atmosphere, sea ice, and ocean resulting form the annular mode. *J. Climate*, **15**, 3043-3057.

Josey, S. A., E. C. Kent, and P. K. Taylor, 1998: The Southampton Oceanography Centre (SOC) Ocean–Atmosphere Heat, Momentum and Freshwater Flux Atlas. Southampton Oceanography Centre Rep. 6, Southampton, United Kingdom, 30 pp. [Available online at http://www.soc.soton.ac.uk/JRD/MET/PDF/soc_flux_atlas.pdf.].

Josey, S.A., 2001: A Comparison of ECMWF, NCEP–NCAR, and SOC Surface Heat Fluxes with Moored Buoy Measurements in the Subduction Region of the Northeast Atlantic. *J. Climate*, **14**, 1780–1789.

Kalnay, E., M. Kanamitsu, R. Kistler, W. Collins, D. Deaven, L. Gandin, M. Iredell, S. Saha, G. White, J. Woollen, Y. Zhu, A. Leetmaa, B. Reynolds, M. Chelliah, W. Ebisuzaki, W. Higgins, J. Janowiak, K. Mo, C. Ropelewski, J. Wang, R. Jenne, and D. Joseph, 1996: The NCEP/NCAR 40-Year Reanalysis Project. *Bull. Amet. Soc.,* **77**, 437–471.

Kushnir, Y., 1994: Interdecadal Variations in North Atlantic Sea Surface Temperature and Associated Atmospheric Conditions. *J. Climate*, **7**, 141–157.

Lau, N.-C. and M. J. Nath, 1996: The role of the 'atmospheric bridge' in linking tropical Pacific ENSO events to extratropical SST anomalies. *J. Climate*, **9,** 2036-2057

L'Heureux, M.L., and D.W.J. Thompson, 2006: Observed Relationships between the El Niño–Southern Oscillation and the Extratropical Zonal-Mean Circulation. *J. Climate*, **19**, 276–287.

Lorenz, D.J., and D.L. Hartmann, 2001: Eddy–Zonal Flow Feedback in the Southern Hemisphere. *J. Atmos. Sci.*, **58**, 3312–3327.

Lorenz, D.J., and D.L. Hartmann, 2003: Eddy–Zonal Flow Feedback in the Northern Hemisphere Winter. *J. Climate*, **16**, 1212–1227.

Lovenduski, N. S., and N. Gruber, 2005: Impact of the Southern Annular Mode on Southern Ocean circulation and biology. *Geophys. Res. Lett.*, **32**, doi:10.1029/2005GL022727**.**

Luksch, U., 1996: Simulation of North Atlantic Low-Frequency SST Variability . *J. Climate*, **9**, 2083–2092.

Marshall, J., Kushnir, Y., Battisti, D., Chang, P., Czaja, A., Dickson, R., McCartney, M., Saravanan, R., and Visbeck, M., 2001: North Atlantic Climate Variability: phenomena, impacts and mechanisms. *Inter. Jour. Climatology*, **21**, 1863-1898

Namias, J., and R. M. Born, 1970: Temporal coherence in North Pacific sea-surface temperature patterns. *J. Geophys. Res.*, **75,** 5952-5955.

Namias, J., and R. M. Born, 1974: Further studies of temporal coherence in North Pacific sea surface temperatures. *J. Geophys. Res*., **79**, 797-798.

Namias, J., X. Yuan, and D.R. Cayan, 1988: Persistence of North Pacific Sea Surface Temperature and Atmospheric Flow Patterns. *J. Climate*, **1**, 682–703.

Norris, J.R., Y. Zhang, and J.M. Wallace, 1998: Role of Low Clouds in Summertime Atmosphere–Ocean Interactions over the North Pacific. *J. Climate*, **11**, 2482–2490.

Park, S., C. Deser, and M.A. Alexander, 2005: Estimation of the Surface Heat Flux Response to Sea Surface Temperature Anomalies over the Global Oceans. *J. Climate*, **18**, 4582–4599.

Park, S., M. A. Alexander, and C. Deser, 2006: The impact of cloud radiative feedback, remote ENSO forcing, and entrainment on the persistence of North Pacific sea

surface temperature anomalies. *J. Climate,* **19**, 6243–6261.

Reynolds, R.W., N.A. Rayner, T.M. Smith, D.C. Stokes, and W. Wang, 2002: An Improved In Situ and Satellite SST Analysis for Climate. *J. Climate*, **15**, 1609–1625.

Screen J.A., Gillett N.P., Karpechko A.Y., Stevens D.P., 2009: Mixed layer temperature response to the Southern Annular Mode: mechanisms and model representation. Journal of Climate: In Press

Seager, R., Y. Kushnir, M. Visbeck, N. Naik, J. Miller, G. Krahmann, and H. Cullen, 2000: Causes of Atlantic Ocean Climate Variability between 1958 and 1998. *J. Climate*, **13**, 2845–2862.

Sen Gupta, A., and M. H. England, 2006: Coupled ocean-atmosphere-ice response to variations in the Southern Annular Mode. *J. Climate,* **19**, 4457-4486.

Smith, S.R., D.M. Legler, and K.V. Verzone, 2001: Quantifying Uncertainties in NCEP Reanalyses Using High-Quality Research Vessel Observations. *J. Climate*, **14**, 4062–4072.

Sura, P., M. Newman, and M. A. Alexander, 2006: Daily to decadal sea surface temperature variability driven by state-dependent stochastic heat fluxes. *J. Phys. Oceanogr.,* **36**, 1940-1958.

Sura, P., and M. Newman, 2008: The impact of rapid wind variability upon air-sea thermal coupling. *J. Climate*, **21**, 621-637.

Thompson, D.W.J., and J.M. Wallace, 2000: Annular Modes in the Extratropical Circulation. Part I: Month-to-Month Variability. *J. Climate*, **13**, 1000–1016.

Timlin, M.S., M.A. Alexander, and C. Deser, 2002: On the reemergence of North Atlantic SST anomalies., *J. Climate*, **15**, 2707–2712.

Verdy, A., J. Marshall, and A. Czaja, 2006: Sea surface temperature variability along the path of the Antarctic Circumpolar Current. *J. Phys. Oceanography*, **36**, 1317-1331.

Visbeck, M., E. P. Chassignet, R. G. Curry, T. L. Delworth, R. R. Dickson, and G. Krahmann, 2003: The Ocean's Response to North Atlantic Oscillation Variability. The North Atlantic Oscillation: Climatic Significance and Environmental Impact, J. W. Hurrell, Y. Kushnir, G. Ottersen, M. Visbeck, American Geophysical Union, 113-146.

Watanabe, M. and M. Kimoto, 2000: On the persistence of decadal SST anomalies in the North Atlantic. *J. Climate*, **13**, 3017-3028.

Yu, L., R.A. Weller, and B. Sun, 2004: Mean and Variability of the WHOI Daily Latent and Sensible Heat Fluxes at In Situ Flux Measurement Sites in the Atlantic Ocean. *J. Climate*, **17**, 2096–2118.

Zhang, Y., J.R. Norris, and J.M. Wallace, 1998: Seasonality of Large-Scale Atmosphere–Ocean Interaction over the North Pacific. *J. Climate*, **11**, 2473–2481.

Figure Captions

Figure 1. Regressions of weekly-mean sea surface temperature anomalies (°C) onto the (left) Northern Annular Mode and (right) Southern Annular Mode. Individual black boxes denote the smaller scale regions analyzed in Section 3 (see text for details).

Figure 2. Autocorrelation functions of the expansion coefficient time series of the observed (top) year-round and (bottom) hemisphere warm (dashed) and cold (solid) season SST pattern associated with the SAM (black) and the NAM (blue). Correlations exceeding 0.4 are statistically significant at the 95% confidence level (short dashed black line).

Figure 3. Autocorrelation functions of the expansion coefficient time series of the observed cold season SST pattern associated with the SAM (solid black) and the NAM (solid blue). The dashed lines correspond to the solutions to Eq. (2) for ρ=1000 kg m^{-3}, c_p=4218 J kg^{-1} K^{-1}, λ= 25 Wm^{-2} K^{-1}, and mixed layer depths of H=115 m (black dashed) and H=75m (blue dashed). The shading corresponds to a range of solutions to Eq. (2) for λ= 20-30 Wm^{-2} K^{-1}.

Figure 4. Autocorrelation functions of the expansion coefficient time series of the observed cold season SST pattern associated with the SAM (solid black) and the NAM (solid blue). The dashed lines correspond to the autocorrelations of the solutions to Eq. (1) for ρ=1000 kg m^{-3}, c_p=4218 J kg^{-1} K^{-1}, λ= 25 Wm^{-2} K^{-1}. F is given as the observed surface turbulent + Ekman heat fluxes associated with the SAM and NAM, and mixed

layer depths of H=115 m (black dashed) and H=75 m (blue dashed). The shading corresponds to a range of solutions to Eq. (1) for λ= 20-30 Wm^{-2} K^{-1}.

Figure 5. Autocorrelations of observed area-averaged cold season SST anomalies (solid blue), T' derived from the observed heat flux model in Eq. (1) (dashed blue line) and T' derived from the white noise model in Eq. (2) (dashed red line) for the (top) subpolar North Atlantic, (middle) Sargasso Sea and (bottom) subtropical North Atlantic. The shading corresponds to a range of solutions to Eq. (1) for λ= 20-30 Wm^{-2} K^{-1} for each region.

Figure 6. Autocorrelations of observed area- averaged cold season SST anomalies (solid black), T' derived from the observed heat flux model in Eq. (1) (dashed black line) and T' derived from the white noise model in Eq. (2) (dashed red line) for the (top left) central South Pacific, (bottom left) western South Pacific, (top right) central Indian Ocean and (bottom right) South Atlantic. The shading corresponds to a range of solutions to Eq. (1) for λ= 20-30 Wm^{-2} K^{-1} for each region.

Figure 7. Autocorrelation functions of the expansion coefficient time series of the cold season (top) surface turbulent (middle) Ekman heat and (bottom) turbulent+Ekman heat flux patterns associated with the cold season SAM (black) and NAM (blue). Correlations exceeding +/- 0.1 are statistically significant at the 95% confidence level (short dashed line).

Figure 8. Monthly mean cold season surface turbulent+Ekman flux (shading) and Z1000 (contours) anomalies regressed onto monthly values of the NAM index at (top) +1 week (NAM leads), (second from top) 3 weeks, (middle) 5 weeks, (second from bottom) 7 weeks and (bottom) 9 weeks. Positive heat fluxes are directed into the ocean and are given in Wm-2. Positive (negative) contours correspond to solid (dashed) lines of Z1000 and are drawn at 3, 6, 9...m. The green contours denote regions of heat flux anomalies that exceed the 95% confidence level.

Figure 9. As in Figure 8 but regressions are now based on the SAM index.

Figure 10. Relationship between the e-folding time scale of atmospheric forcing (F') constructed from a 1st Order Markov model and the e-folding time scale of the solution to Eq. (1) for ρ=1000 kg m^{-3}, c_p=4218 J kg^{-1} K^{-1}, for λ= 25 Wm^{-2} K^{-1} and H=75m. See text for details.

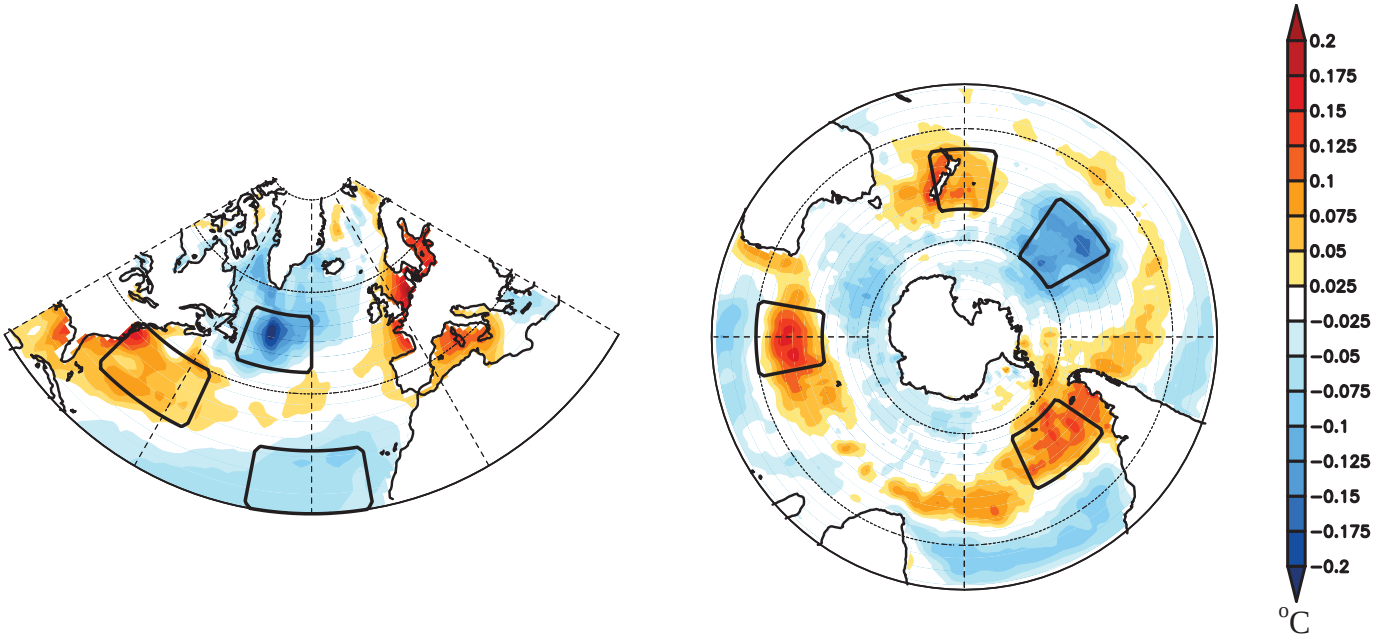

Figure 1. Regressions of weekly-mean sea surface temperature anomalies (^{o}C) onto the (left) Northern Annular Mode and (right) Southern Annular Mode. Individual black boxes denote the smaller scale regions analyzed in Section 3 (see text for details).

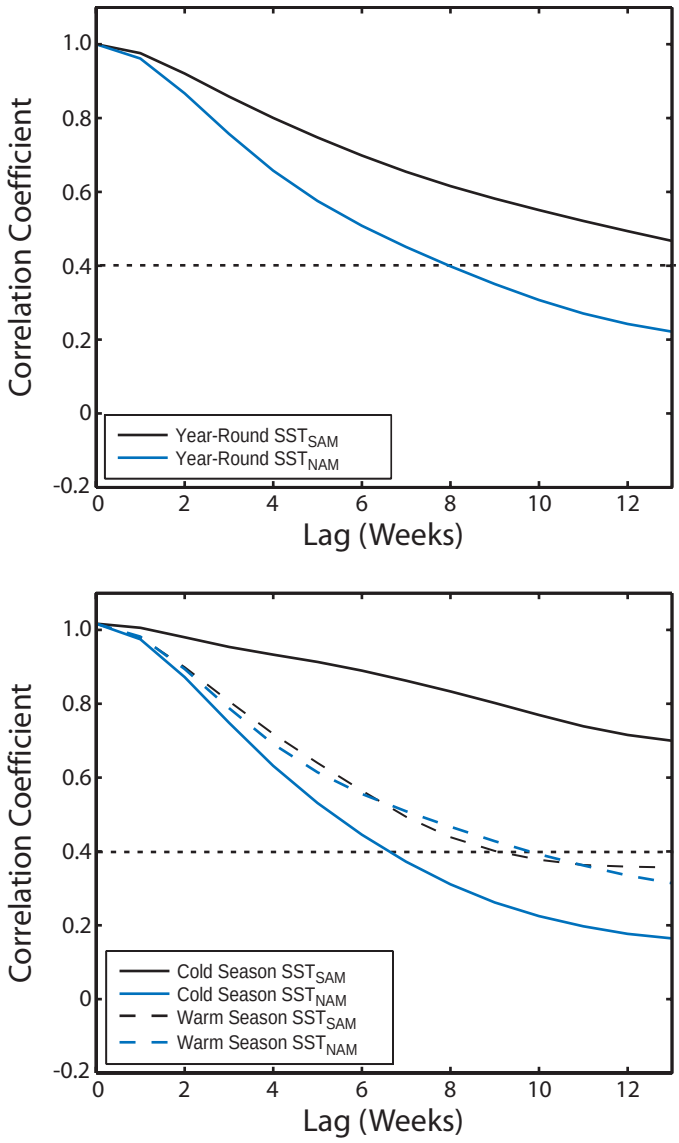

Figure 2. Autocorrelation functions of the expansion coefficient time series of the observed (top) year-round and (bottom) hemisphere warm (dashed) and cold (solid) season SST pattern associated with the SAM (black) and the NAM (blue). Correlations exceeding 0.4 are statistically significant at the 95% confidence level (short dashed black line).

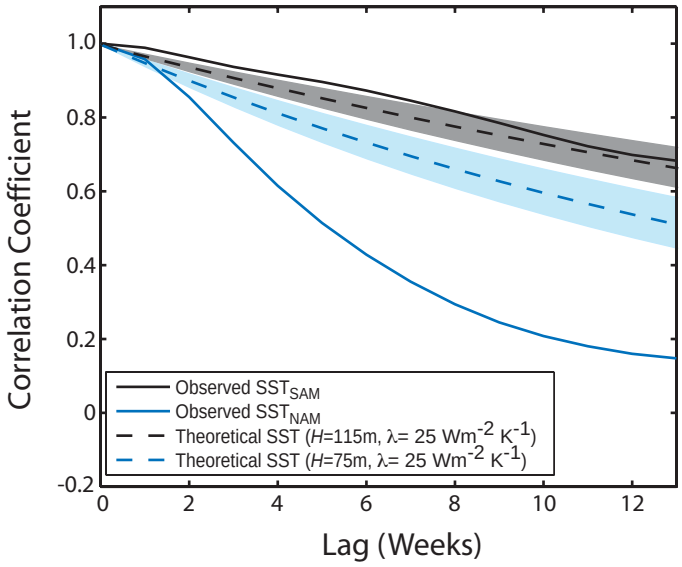

Figure 3. Autocorrelation functions of the expansion coefficient time series of the observed cold season SST pattern associated with the SAM (solid black) and the NAM (solid blue). The dashed lines correspond to the solutions to Eq. (2) for ρ=1000 kg m^{-3}, c_p=4218 J kg^{-1} K^{-1}, λ= 25 Wm^{-2} K^{-1}, and mixed layer depths of H=115 m (black dashed) and H=75m (blue dashed). The shading corresponds to a range of solutions to Eq. (2) for λ= 20-30 Wm^{-2} K^{-1}.

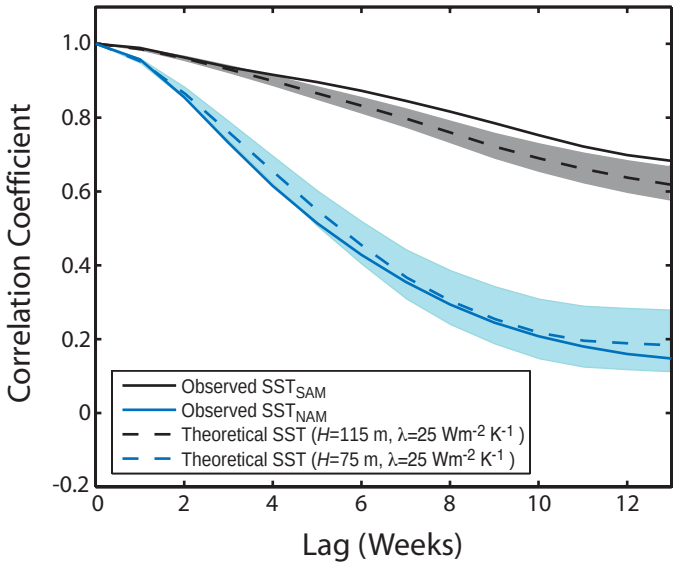

Figure 4. Autocorrelation functions of the expansion coefficient time series of the observed cold season SST pattern associated with the SAM (solid black) and the NAM (solid blue). The dashed lines correspond to the autocorrelations of the solutions to Eq. (1) for ρ=1000 kg m^{-3}, c_p=4218 J kg^{-1} K^{-1}, λ= 25 Wm^{-2} K^{-1}. F is given as the observed surface turbulent + Ekman heat fluxes associated with the SAM and NAM, and mixed layer depths of H=115 m (black dashed) and H=75 m (blue dashed). The shading corresponds to a range of solutions to Eq. (1) for λ= 20-30 Wm^{-2} K^{-1}.

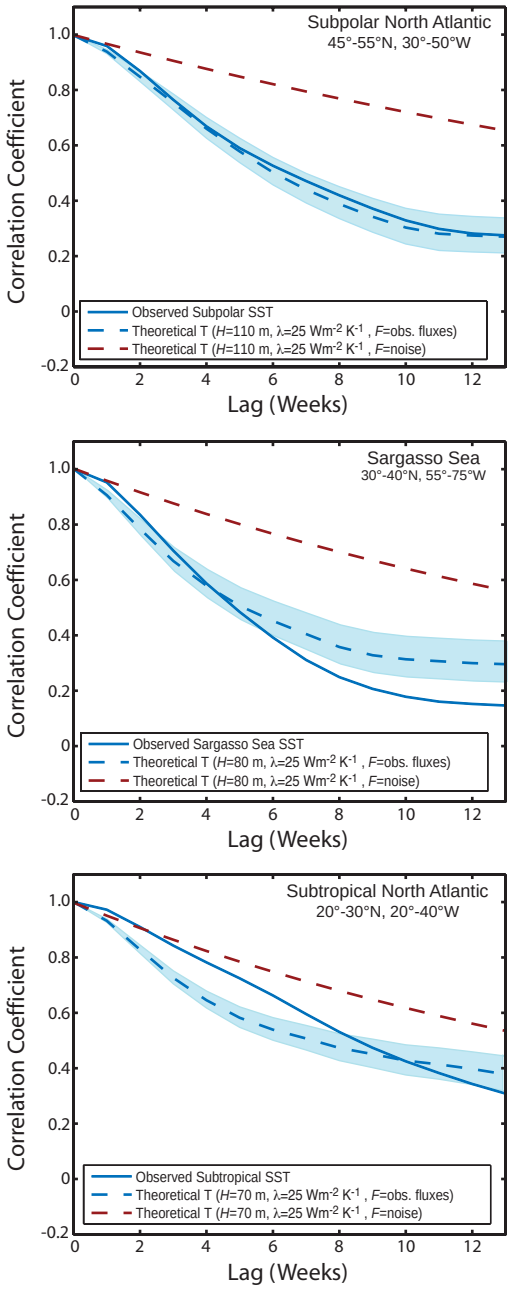

Figure 5. Autocorrelations of observed area-averaged cold season SST anomalies (solid blue), *T'* derived from the observed heat flux model in Eq. (1) (dashed blue line) and *T'* derived from the white noise model in Eq. (2) (dashed red line) for the (top) subpolar North Atlantic, (middle) Sargasso Sea and (bottom) subtropical North Atlantic. The shading corresponds to a range of solutions to Eq. (1) for λ= 20-30 Wm^{-2} K^{-1} for each region.

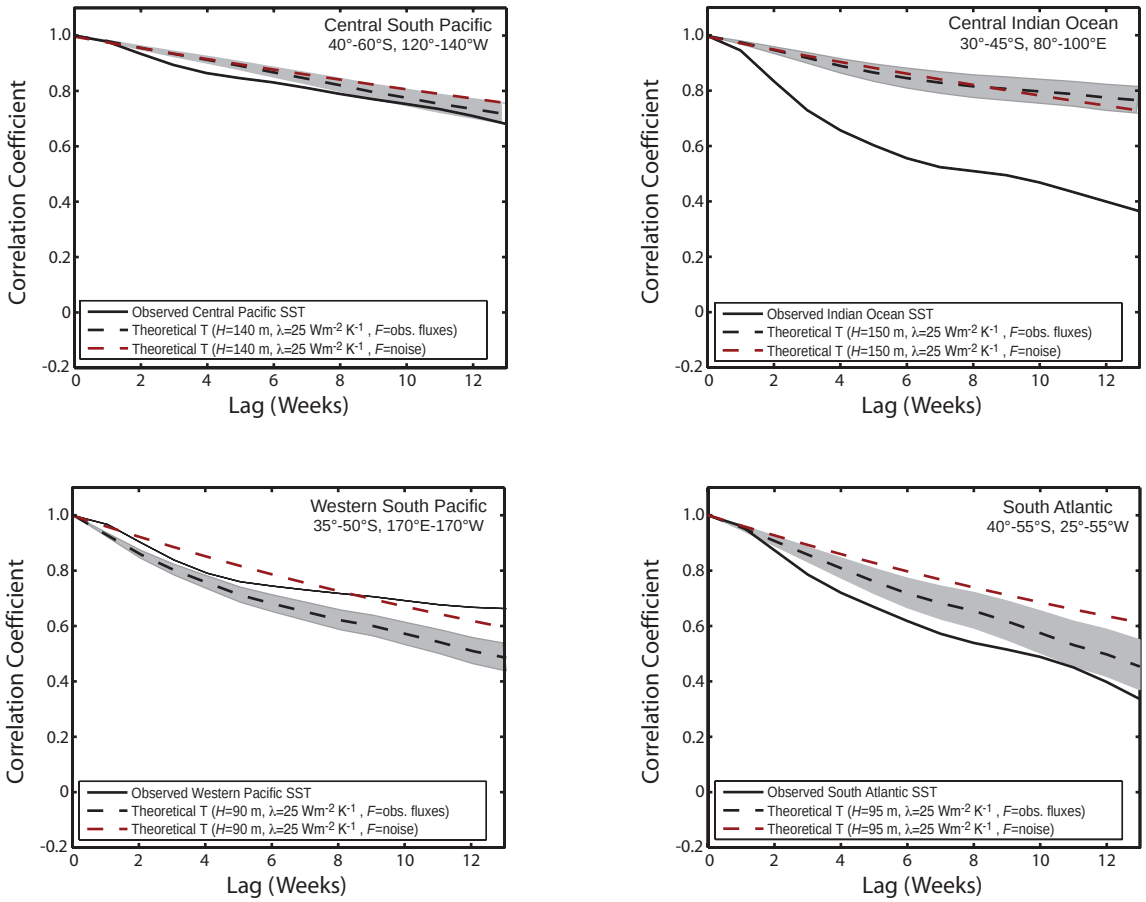

Figure 6. Autocorrelations of observed area- averaged cold season SST anomalies (solid black), *T'* derived from the observed heat flux model in Eq. (1) (dashed black line) and *T'* derived from the white noise model in Eq. (2) (dashed red line) for the (top left) central South Pacific, (bottom left) western South Pacific, (top right) central Indian Ocean and (bottom right) South Atlantic. The shading corresponds to a range of solutions to Eq. (1) for λ= 20-30 Wm^{-2} K^{-1} for each region.

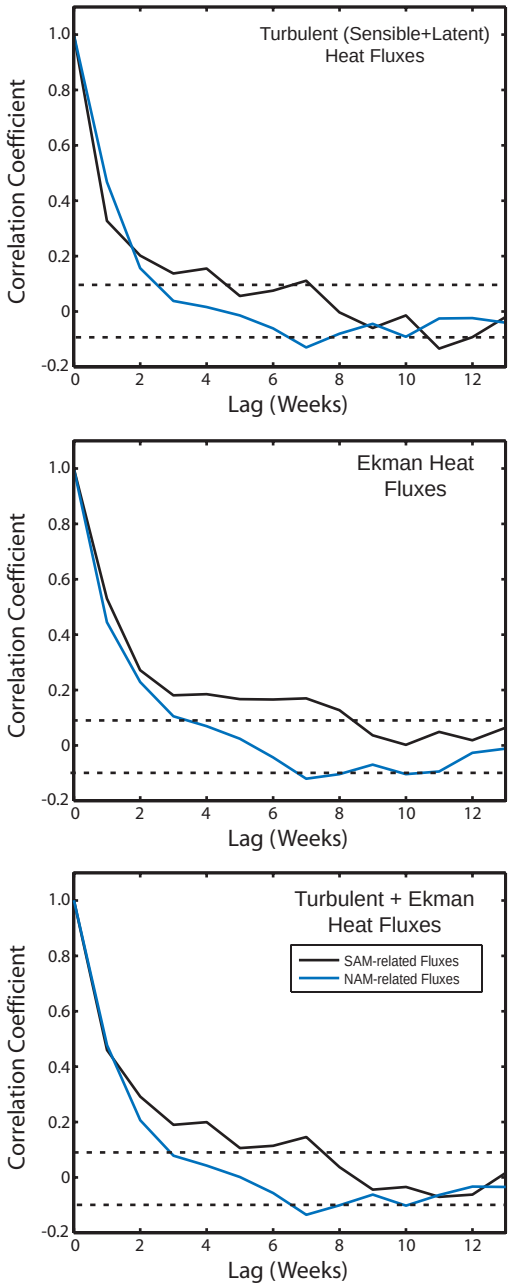

Figure 7. Autocorrelation functions of the expansion coefficient time series of the cold season (top) surface turbulent (middle) Ekman heat and (bottom) turbulent+Ekman heat flux patterns associated with the cold season SAM (black) and NAM (blue). Correlations exceeding +/- 0.1 are statistically significant at the 95% confidence level (short dashed line).

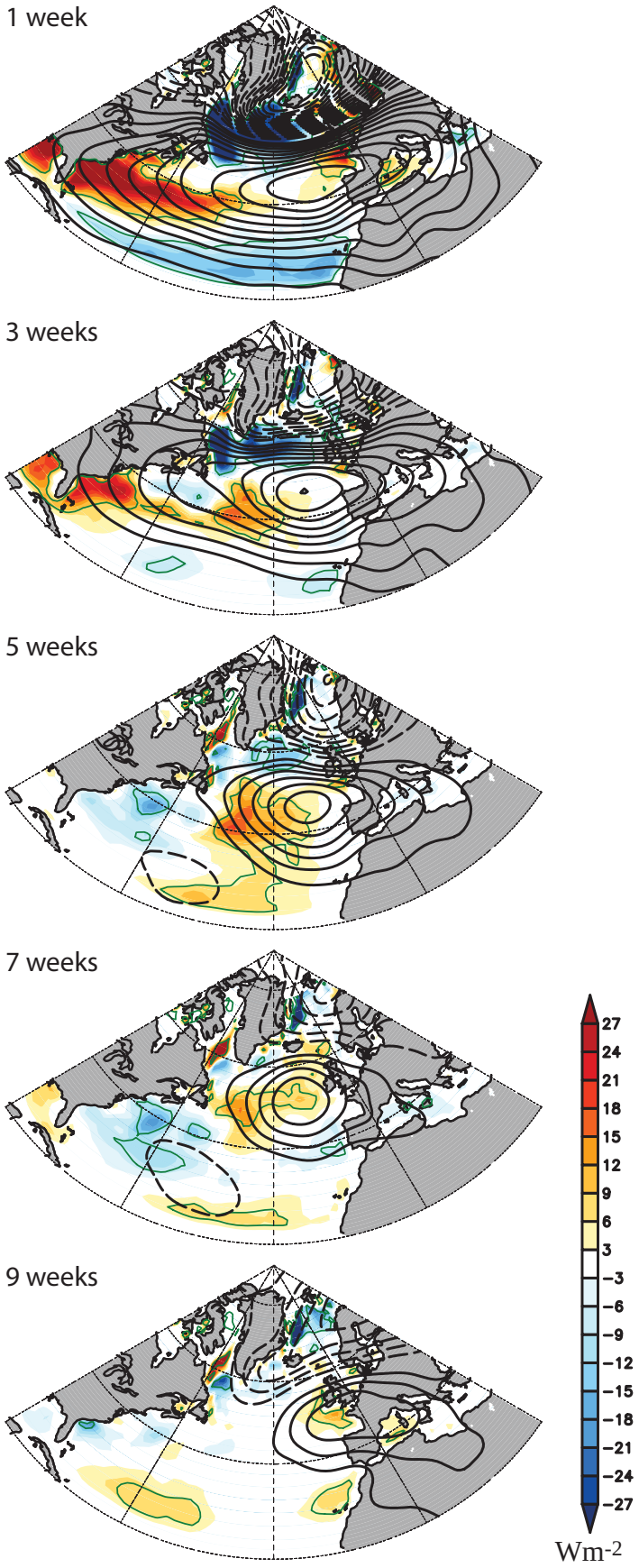

Figure 8. Monthly mean cold season surface turbulent+Ekman flux (shading) and Z_{1000} (contours) anomalies regressed onto monthly values of the NAM index at (top) +1 week (NAM leads), (second from top) 3 weeks, (middle) 5 weeks, (second from bottom) 7 weeks and (bottom) 9 weeks. Positive heat fluxes are directed into the ocean and are given in Wm^{-2}. Positive (negative) contours correspond to solid (dashed) lines of Z_{1000} and are drawn at 3, 6, 9...m. The green contours denote regions of heat flux anomalies that exceed the 95% confidence level.

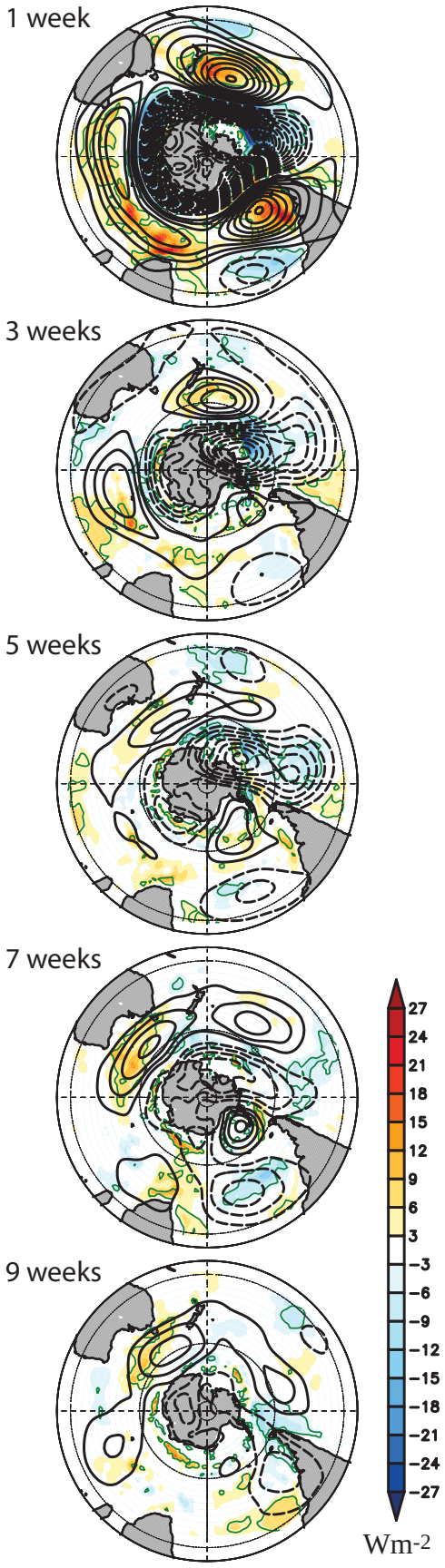

Figure 9. As in Figure 8 but regressions are now based on the SAM index.

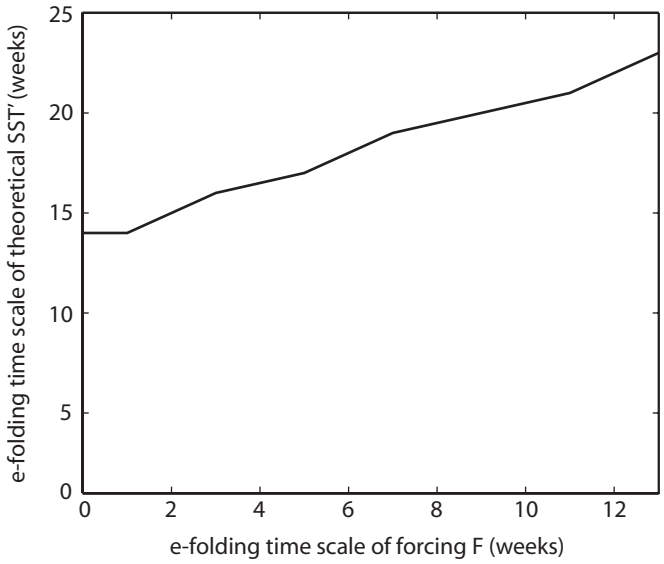

Figure 10. Relationship between the e-folding time scale of atmospheric forcing (F') constructed from a 1st Order Markov model and the e-folding time scale of the solution to Eq. (1) for ρ=1000 kg m^{-3}, c_p=4218 J kg^{-1} K^{-1}, λ= 25 Wm^{-2} K^{-1} and H=75m. See text for details.